INSTITUTE OF PHYSICS PUBLISHING MEASUREMENT SCIENCE AND TECHNOLOGY

Meas. Sci. Technol. **17** (2006) 3245–3249 doi:10.1088/0957-0233/17/12/007

Photopyroelectric calorimetry down to 10 K

M Massot, A Oleaga and A Salazar

Departamento de Física Aplicada I, Escuela Técnica Superior de Ingeniería, Universidad del País Vasco, Alameda Urquijo s/n, 48013 Bilbao, Spain

Received 29 August 2006, in final form 19 September 2006
Published 3 November 2006
Online at stacks.iop.org/MST/17/3245

Abstract

In photopyroelectric calorimetry thermal conductivity, thermal diffusivity and specific heat are measured simultaneously from the same heating or cooling run. As it provides a good signal-to-noise ratio with small temperature gradients, it is well suited to study the critical behaviour of phase transitions. Up to now, it has been mainly used above 77 K. In this work we implement the cryogenic set-up to work down to 10 K. The troubles introduced by the cryostat vibrations and by the freezing of the coupling grease are analysed. This set-up has been used to characterize the critical parameters of the antiferromagnetic $SmMnO_3$, which agree with the three-dimensional XY universality class.

Keywords: photopyroelectric, phase transitions, critical behaviour, thermal properties, manganites

1. Introduction

Photopyroelectric (PPE) calorimetry has been widely used to measure the thermal properties of solids and liquids (see [1] and references therein). In the standard back configuration, where an opaque sample is periodically illuminated on one side while the other side is in contact with the pyroelectric detector, the thermal parameters can be obtained from simple linear relations. In particular, when both sample and pyroelectric detector are thermally thick the natural logarithm of the amplitude and the phase of the PPE signal are parallel straight lines when represented as a function of the square root of the modulation frequency. From their slope and from the vertical separation, thermal diffusivity (D) and thermal effusivity ($e = \sqrt{\rho c K}$) are obtained, respectively. Then, from the constitutive relation ($K = \rho c D$, where ρ is the density), thermal conductivity (K) and specific heat (c) can be retrieved [2, 3]. PPE calorimetry has two main advantages: on the one hand, the temperature dependence of D, K and c can be obtained from one single heating and/or cooling run at a fixed frequency; on the other hand, a good signal-to-noise ratio is obtained with very small light intensities. This means that small temperature gradients are induced in the sample and therefore this calorimetry is especially suited to studying phase transitions [4]. In the last years we have been using a PPE calorimeter, based on a nitrogen bath cryostat, to characterize the thermal properties of magnetic samples around their transition temperature down to 77 K [5, 6].

In this paper we present a recent development of PPE calorimetry in order to measure the thermal properties around phase transitions down to 10 K. PPE measurements down to 20 K have already been published [7]. However, the minimal cooling/heating rate of 1 K min^{-1} was too fast to observe the details of the phase transitions in the critical region. In our PPE set-up the minimal cooling/heating rate is 5 mK min^{-1} and therefore high resolution measurements in the near vicinity of the transition temperature are allowed. We have used an actively cooled cryostat that uses mechanical devices to cool materials to cryogenic temperatures. Its main advantage is that it uses helium gas as the working fluid instead of the very expensive liquid helium, but it presents some drawbacks when used in PPE measurements. On the one hand, the vibrations generated by the cooler are transmitted to the cold finger and affect the PPE signal since the pyroelectric sensor is piezoelectric as well. Moreover, as the temperature decreases the thermal coupling between the sample and the pyroelectric sensor is reduced and therefore the thermal diffusivity is underestimated while the specific heat is overestimated. After overcoming these drawbacks we have performed high resolution measurements in the antiferromagnetic $SmMnO_3$ around the Néel temperature $T_N = 59$ K. The critical parameters obtained ($\alpha = -0.012$ and $A'/A = 1.02$) agree with the three-dimensional XY universality class.

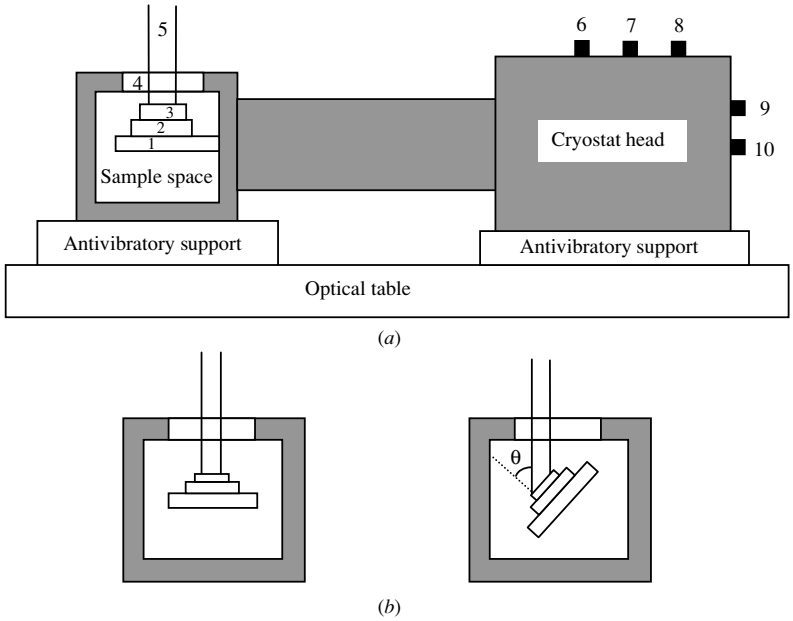

Figure 1. Scheme of the cryogenic set-up. (1) cold finger, (2) pyroelectric detector, (3) sample, (4) optical window, (5) heating laser, (6) photopyroelectric signal, (7) to the vacuum pump, (8) to the temperature controller, (9) High pressure He input, (10) Low pressure He output. (*a*) Side view, (*b*) front view.

2. Experimental set-up and calibration

The experimental set-up is based on a cell modification of a PPE calorimeter used in the back configuration [1]. An acousto-optically modulated He–Ne laser beam of 5 mW illuminates the upper surface of the sample under study. Its rear surface is in thermal contact with a 350 μm thick $LiTaO_3$ pyroelectric detector with Ni–Cr electrodes on both faces, by using an extremely thin layer of a high heat-conductive silicone grease (Dow Corning, 340 Heat Sink Compound). The photopyroelectric signal is processed by a lock-in amplifier in the current mode. Both the sample and the detector are placed in contact with the cold finger of an actively cooled helium cryostat (Oxford Instruments, OptistatAC-V 01). It uses a Gifford-McMahon refrigerator which works as follows. The compressor system supplies compressed helium to the cold head through flexible metal hoses. The gas expands in the cryostat unit to provide refrigeration, by expanding the high-pressure helium to low pressure, and then returns to the compressor unit. The cold head exchanger is in good thermal contact with the sample holder. A scheme of the cryogenic system is shown in figure 1. This system allows measurements in the temperature range from 10 K to 325 K at rates that vary from 100 mK min^{-1} for measurements on a wide temperature range to 5 mK min^{-1} for high resolution runs close to phase transitions. Measurements were performed at 17.0 Hz. This frequency is high enough to guarantee that the pyroelectric sensor is thermally thick in the whole temperature range analysed, but it is low enough to have a high PPE signal. The thicknesses of the samples have been selected to fit the thermally thick requirement.

Besides saving the very expensive liquid helium, the main advantage of this cryogenic system is that it allows long cooling/heating runs which are of practical interest in phase transition measurements. However, it introduces some troubles that must be overcome for use in PPE calorimetry. The first one is related to the vibrations produced by the cryostat head that are transmitted by the sample holder to the pyroelectric detector. As this last one is also piezoelectric an additional signal is superimposed to the pyroelectric one. In figure 2 the signal amplitude is recorded as a function of the frequency in the absence of illumination. Since the cryostat head rotates at a rate of one revolution per second, even frequencies produce high intensity signals of piezoelectric nature due to resonance. Therefore these frequencies must be avoided in this PPE calorimeter.

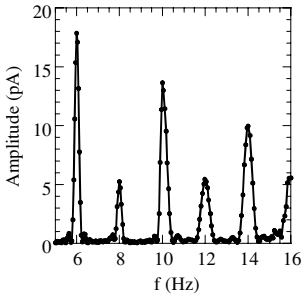

Figure 2. Piezoelectric signal induced by the cryostat vibrations in the absence of heating light.

An additional source of piezoelectric contribution is related to the orientation of the sample holder (see figure 1(*b*)). We have analysed its influence on the residual noise in the absence of heating illumination. From 325 K down to 240 K this residual noise is independent of the orientation of the sample holder and small enough to be neglected (≈0.3%). However, as the temperature drops below 240–230 K, i.e. the freezing temperature of the coupling grease, this residual noise of piezoelectric nature depends dramatically on the sample holder orientation. When the sample is horizontal ($\theta = 0^\circ$),

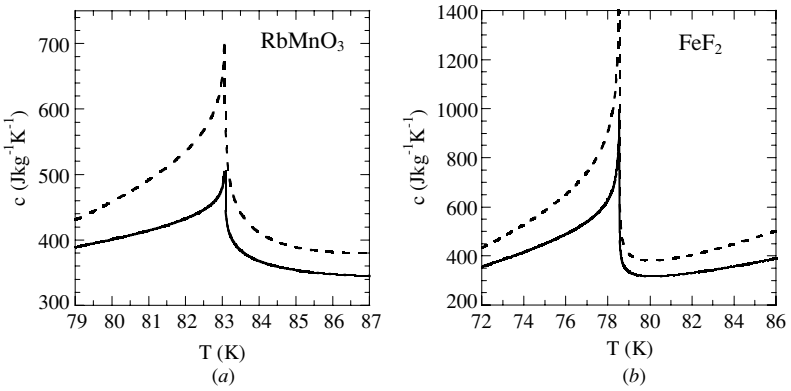

Figure 3. Critical behaviour of specific heat (*a*) in $RbMnF_3$, a 3D-Heisenberg antiferromagnet and (*b*) in FeF_2, a 3D-Ising antiferromagnet. The continuous line represents the ideal specific heat. The dotted line represents the overestimated specific heat obtained in PPE calorimetry due to the presence of the grease layer between the sample and the detector.

as is shown on the left side of figure 1(*b*), measurements are not possible because of a noise of about 100%. As the angle of the sample holder (θ) increases the noise is clearly reduced. For instance, in measurements performed at 50 K and with an integration time of 2 s for $\theta = 22.5^\circ$, 45° and 67.5°, the noise is 10%, 2.5% and 1% respectively ($\theta = 90^\circ$ was not suitable for mechanical stability). Accordingly, all measurements have been performed at $\theta = 67.5^\circ$.

The coupling grease introduces another problem. It has been already demonstrated that even if it is extremely thin it increases the slope of the linearity of the natural logarithm of the amplitude ($\ln V$) and that of the phase (Ψ) of the PPE signal when represented as a function of the square root frequency [8]. As a consequence, the thermal diffusivity of solid samples is underestimated, and this effect is higher for high thermal diffusivity samples. On the other hand, the vertical separation of both straight lines remains almost unaffected and consequently the thermal effusivity is accurately measured. Taking into account that $K = e\sqrt{D}$ and $c = \frac{e}{\rho\sqrt{D}}$, it is concluded that the thermal conductivity is underestimated and the specific heat is overestimated. These results have been confirmed in room temperature measurements [8]. However, at low temperatures, since the coupling grease solidifies, the thermal coupling between the sample and the pyroelectric sensor becomes worse. This means that the effective thermal properties of this intermediate layer between the sample and the sensor are reduced and therefore the effect of under/overestimation of the thermal properties is enhanced. As we are interested in characterizing the thermal properties of second-order magnetic transitions, we analyse how the mentioned problem affects the determination of the critical parameters. The critical behaviour of the specific heat is described by a function of the form

$$c = B + Ct + A|t|^{-\alpha}(1 + E|t|^{0.5}) \tag{1}$$

where $t = (T - T_C)/T_C$ is the reduced temperature, T_C is the critical temperature, and α, A, B, C and E are adjustable parameters for $T < T_C$. The same equation is used for $T > T_C$ with prime parameters. The linear term represents the background contribution to the specific heat and satisfies $B = B'$ and $C = C'$. The last term is the magnetic contribution to the specific heat with $\alpha = \alpha'$. The term $(1 + E|t|^{0.5})$ is the correction to scaling that represents a singular contribution to the leading power as known from experiments and theory [9, 10]. According to the values of the critical exponent α and of the critical amplitude ratio A'/A, different universality classes can be distinguished. In particular, for three-dimensional (3D) magnets two main results are found: (a) the 3D-Heisenberg model for isotropic magnets with $\alpha = -0.11$ and $A'/A = 1.50$ and (b) the 3D-Ising model for uniaxial magnets with $\alpha = +0.11$ and $A'/A = 0.50$. Now we analyse the influence of the overestimation of the specific heat in PPE experiments due to the coupling grease on the critical parameters of 3D-Heisenberg and 3D-Ising magnets.

In figure 3(*a*) we show the specific heat of $RbMnF_3$, a well-known isotropic antiferromagnet that satisfies a 3D-Heisenberg model [11]. The continuous line represents the ideal specific heat that satisfies $\alpha = -0.11$ and $A'/A = 1.50$. The dotted line represents the overestimated specific heat due to the presence of the grease layer between the sample and the detector. Calculations have been performed using the expression for the normalized PPE signal for the thermally thick sample and the pyroelectric detector that incorporates the effect of the coupling grease [8]

$$V_n = \frac{4\exp(-\sigma_s \ell_s)}{(1+b_{sg})(1+b_{gp})\exp(\sigma_g \ell_g)+(1-b_{sg})(1-b_{gp})\exp(-\sigma_g \ell_g)}, \tag{2}$$

where $b_{ij} = e_i/e_j$, $\sigma_i = \frac{(1+i)}{\mu_i}$, $\mu_i = \sqrt{\frac{D_i}{\pi f}}$ being the thermal diffusion length. The subindices s, p and g stand for sample, pyroelectric detector and grease, respectively. The following data have been used: $l_s = 1.0$ mm, D_s (79 K) = 8.5 mm^2 s^{-1}, e_s (79 K) = 4900 J m^{-2} K^{-1} s$^{-1/2}$, $l_g = 10$ μm, D_g = 0.10 mm^2 s^{-1}, e_g = 500 J m^{-2} K^{-1} s$^{-1/2}$, $l_p = 0.35$ mm, $D_p = 3.0$ mm^2 s^{-1}, $e_p = 2200$ J m^{-2} K^{-1} s$^{-1/2}$. As expected, the influence of the grease layer produces an underestimation of the thermal diffusivity $D'(79\text{ K}) = 6.95$ mm^2 s^{-1}, while the thermal effusivity remains unchanged $e'(79\text{ K}) = e$ (79 K) = 4900 J m^{-2} K^{-1} s$^{-1/2}$. Accordingly, an overestimation of the specific heat is produced $c'(79\text{ K}) = 430$ J kg^{-1} K^{-1}. By repeating this same calculation in the whole range between 79 K and 89 K we obtain the temperature dependence of the apparent specific heat due to the grease, i.e. the dotted line in figure 3(*a*). By fitting this dotted line to equation (1) we find $\alpha = -0.110 \pm 0.004$ and $A'/A = 1.49 \pm 0.01$. This is a very interesting result since it indicates that, even for a high

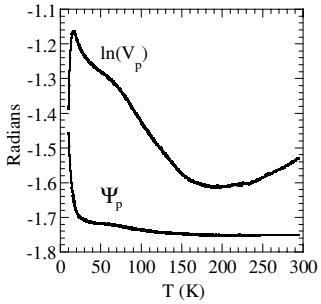

Figure 4. Temperature dependence of the photopyroelectric signal provided by the bare detector.

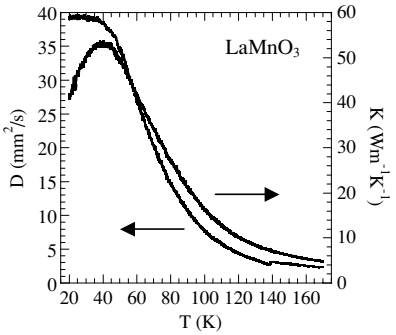

Figure 5. Temperature dependence of the thermal conductivity and thermal diffusivity of $LaMnO_3$.

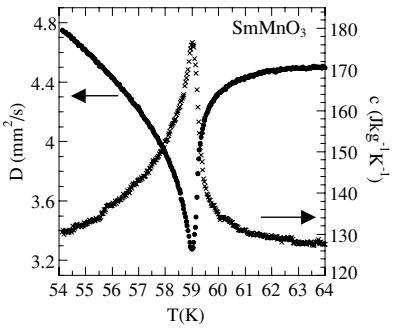

Figure 6. Temperature dependence of the thermal diffusivity and specific heat of $SmMnO_3$ near the Néel temperature.

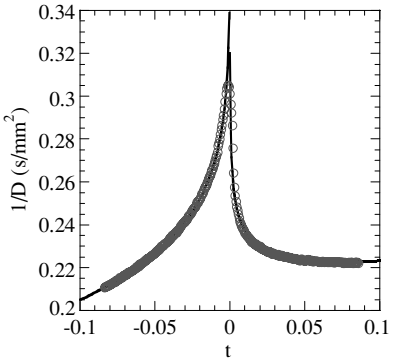

Figure 7. Inverse of the thermal diffusivity of $SmMnO_3$ as a function of the reduced temperature (t) in the near vicinity of the Néel temperature. The open circles are the experimental data and the continuous lines the fitted functions.

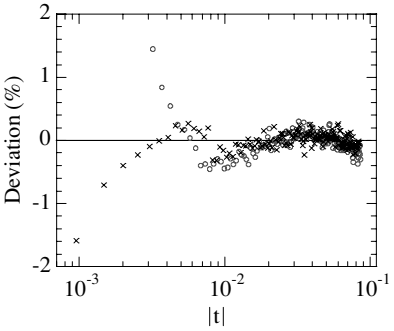

Figure 8. Deviation plots corresponding to the fit of figure 7. Open circles are for $T < T_N$ and crosses for $T > T_N$.

overestimation of the specific heat produced by an unrealistic thick grease layer, the critical parameters are obtained with high accuracy.

Similar calculations have been performed for FeF_2, a 3D-Ising antiferromagnet [12]. In figure 3(*b*) the continuous line represents the ideal specific heat that satisfies $\alpha = +0.11$ and $A'/A = 0.50$. The dotted line represents the specific heat calculated from equation (2) using the following data: $l_s = 1.0$ mm, $D_s(72\ \mathrm{K}) = 22.0\ \mathrm{mm^2\ s^{-1}}$, $e_s(72\ \mathrm{K}) = 6665\ \mathrm{J\ m^{-2}\ K^{-1}\ s^{-1/2}}$, $l_g = 10\ \mu$m, $D_g(72\ \mathrm{K}) = 0.10\ \mathrm{mm^2\ s^{-1}}$, $e_g(72\ \mathrm{K}) = 500\ \mathrm{J\ m^{-2}\ K^{-1}\ s^{-1/2}}$, $l_p = 0.35$ mm, $D_p(72\ \mathrm{K}) = 3.1\ \mathrm{mm^2\ s^{-1}}$, $e_p(72\ \mathrm{K}) = 2150\ \mathrm{J\ m^{-2}\ K^{-1}\ s^{-1/2}}$. The influence of the grease layer produces an underestimation of the thermal diffusivity $D'(72\ \mathrm{K}) = 14.8\ \mathrm{mm^2\ s^{-1}}$, while the thermal effusivity remains unchanged $e'(72\ \mathrm{K}) = e(72\ \mathrm{K}) = 6665\ \mathrm{J\ m^{-2}\ K^{-1}\ s^{-1/2}}$. Accordingly, an overestimation of the specific heat is produced $c'(72\ \mathrm{K}) = 432\ \mathrm{J\ kg^{-1}\ K^{-1}}$. By repeating this same calculation in the whole range between 72 K and 85 K we obtain the temperature dependence of the apparent specific heat due to the grease, i.e. the dotted line in figure 3(*b*). By fitting this dotted line to equation (1) we find $\alpha = +0.111 \pm 0.002$ and $A'/A = 0.505 \pm 0.007$. As before, the critical parameters are almost unaffected by the influence of the grease layer.

3. Experimental results and discussion

In figure 4 the temperature dependence of the natural logarithm of the amplitude ($\ln V_p$) and that of the phase (Ψ_p) of the PPE signal provided by the bare pyroelectric detector is shown. This knowledge is of practical interest since in PPE measurements we work with normalized signals, i.e. the ratio of the PPE signal with and without a sample. As is well known, the phase is almost temperature independent above 77 K and therefore normalization is not necessary. However, below this temperature the phase increases as the temperature decreases. For temperatures below 40 K, normalization must be performed carefully since both amplitude and phase change dramatically.

In order to calibrate our low temperature set-up we have measured the temperature dependence of the thermal properties of $LaMnO_3$, which were already measured above 77 K using a nitrogen bath cryostat [6]. We have used a slice 0.35 mm thick that was cut from the grown ingots, perpendicular to the growth direction (c-axis). The

temperature evolution of K and D is shown in figure 5. The results down to 80 K are the same as those obtained with the liquid nitrogen cryostat [6]. Below this temperature the thermal diffusivity increases until it reaches a plateau, that is the expected behaviour for this quantity. In its turn, the thermal conductivity also increases as temperature decreases until it reaches a maximum and then decreases. This is also the expected result for K at low temperatures and is related to the fact that the phonon mean free path reaches a constant value that is determined by the external boundaries of the crystal [13].

As an application of this PPE set-up we have measured the thermal properties of the antiferromagnet $SmMnO_3$ around the Néel temperature. We are interested in measuring the influence of the rare earth substitution on the critical behaviour of $XMnO_3$ (X = La, Pr, Nd, Sm, ...). We have already measured the first three compounds using a liquid nitrogen cryostat [6], but as the Néel temperature of the rest of the family falls below 77 K we need to use the new set-up. The sample we have measured is a single-crystal plate 0.52 mm thick. In figure 6 the temperature dependence of D and c around the transition temperature is shown. Note that D, which is obtained directly from the phase of the PPE signal, is less noisy than c, which is obtained by combining both amplitude and phase. Since the thermal conductivity of $SmMnO_3$ shows no singularity at the transition, the inverse of the thermal diffusivity behaves as the specific heat ($1/D = \rho c/K$) and it has been fitted to the following equation:

$$1/D = G + Ht + F|t|^{-\alpha}(1 + I|t|^{0.5}) \qquad (3)$$

where $t = (T - T_N)/T_N$ is the reduced temperature and G, H, F and I are adjustable parameters for $T < T_N$. The same equation with prime parameters is used for $T > T_N$. In figure 7 the experimental results of $1/D$ are shown by open circles while the continuous line is the best fit to equation (3). The quality of the plot is shown in figure 8. Values for $|t| < 4 \times 10^{-3}$ for $T < T_N$ and for $|t| < 2 \times 10^{-3}$ for $T > T_N$ are affected by rounding and have not been considered in the fit. The critical parameters obtained are $\alpha = -0.012 \pm 0.008$ and $F'/F = 1.02 \pm 0.01$, which agree with the 3D-XY universality class ($\alpha = -0.014$ and $A'/A = 1.06$) [14]. Similar critical parameters are obtained for the specific heat. The fact that $SmMnO_3$ belongs to a different universality class from $LaMnO_3$, $PrMnO_3$ and $NdMnO_3$ could be related to the change from a layered-type (A-type) antiferromagnetic structure to an incommensurate antiferromagnetic structure just for $SmMnO_3$ [15].

In this work we have developed a PPE calorimeter to work below the liquid nitrogen condensing temperature. It has been necessary to overcome some troubles introduced by the vibrations of the cryostat and by the freezing of the coupling grease. This new set-up has been used to measure the critical parameters of the antiferromagnet $SmMnO_3$ that agree with the three-dimensional XY universality class.

Acknowledgments

We thank Massimo Marinelli and Fulvio Mercuri for fruitful discussions. This work has been supported by the University of the Basque Country through research grant no E-15928/2004.

References

[1] Chirtoc M, Dadarlat D, Bicanic D, Antoniow J S and Egée M 1997 *Progress in Photothermal and Photoacoustic Science and Technology* vol 3 ed A Mandelis and P Hess (Bellingham, WA: SPIE)

[2] Marinelli M, Murtas F, Mecozzi M G, Zammit U, Pizzoferrato R, Scudieri F, Martelucci S and Marinelli M 1990 Simultaneous determination of specific heat, thermal conductivity and thermal diffusivity at low temperature via the photopyroelectric technique *Appl. Phys.* A **51** 387–93

[3] Delenclos S, Chirtoc M, Hadj Sahraoui A, Kolinsky C and Buisine J M 2002 Assessment of calibration procedures for accurate determination of thermal parameters of liquids and their temperature dependence using the photopyroelectric method *Rev. Sci. Instrum.* **73** 2773–80

[4] Marinelli M, Zammit U, Mercuri F and Pizzoferrato R 1992 High-resolution simultaneous photothermal measurements of thermal parameters at a phase transition with the pyroelectric technique *J. Appl. Phys.* **72** 1096–100

[5] Oleaga A, Salazar A, Prabhakaran D and Boothroyd A T 2004 Critical behavior of $La_{1-x}Sr_xMnO_3$ ($0 \leqslant x \leqslant 0.35$) by thermal diffusivity measurements *Phys. Rev.* B **70** 184402–8

[6] Oleaga A, Salazar A, Prabhakaran D and Boothroyd A T 2005 Critical behaviour of $RMnO_3$ (R = La, Pr, Nd) by thermal diffusivity and specific heat measurements *J. Phys.: Condens. Matter* **17** 6729–36

[7] Chirtoc M, Giese D, Arnscheidt B, Kalevitch N and Pelzl J 1997 Dual-modulation-frequency photopyroelectric technique: application to thermophysical investigation of $(NH_4)HSO_4$ and $(ND_{42}TeCl_6$ crystals at low temperature *Opt. Eng.* **36** 363–9

[8] Salazar A 2003 On the influence of the coupling fluid in photopyroelectric measurements *Rev. Sci. Instrum.* **74** 825–7

[9] Ahlers G 1980 Critical phenomena at low temperature *Rev. Mod. Phys.* **52** 489–503

[10] Aharony A and Fisher M E 1983 Nonlinear scaling fields and corrections to scaling near criticality *Phys. Rev.* B **27** 4394–400

[11] Marinelli M, Mercuri F, Foglietta S and Belanger D P 1996 Effect of spin-system fluctuations on heat transport in $RbMnF_3$ close to the Néel temperature *Phys. Rev.* B **54** 4087–92

[12] Marinelli M, Mercuri F and Belanger D P 1995 Specific heat, thermal diffusivity, and thermal conductivity of FeF_2 at the Néel temperature *Phys. Rev.* B **51** 8897–903

[13] Berman R 1976 *Thermal Conduction in Solids* (Oxford: Oxford University Press)

[14] Campostrini M, Hasenbusch M, Pelissetto A, Rossi P and Vicari V 2001 Critical behavior of the three-dimensional XY universality class *Phys. Rev.* B **63** 214503–31

[15] Kimura T, Ishihara S, Shintani H, Arima T, Takahashi K T, Ishizaka K and Tokura Y 2003 Distorted perovskite with e^1_g configuration as a frustrated spin system *Phys. Rev.* B **68** 060403(R)–6